A Multi-Channel Electrode for Chronic Recording and Safe Current-Steered Stimulation

Ben Pearre[1,a,¤], Sanne Moorman[1,b], Jun Shen[1,c], Stuart F. Cogan[2,d] Timothy J. Gardner[1,e]

[1] Department of Biology, Boston University, Boston, Massachusetts, United States of America

[2] Department of Bioengineering, University of Texas, Dallas, Texas, United States of America

Author [a] did something, we think. The histology data analysis was by Author [b]. Author [c] performed all surgeries. Authors [b] and [c] did the histologies. Author [d] developed the iridium oxide coating technique. Author [e], the PI, designed and guided the experiment and this paper.

¤ Corresponding author: bwpearre@gmail.com (BP)

Abstract

Electrical control of the brain facilitates a variety of therapeutic and scientific goals, from treating sensory, motor, and cognitive defects to exploring the effects of disrupting or modifying the brain's behaviour in real time. These methods are limited by the brain's immune reaction to foreign matter: over a period of months, glia encapsulate the electrodes, isolating them from neurons. Small electrodes ($< 10\ \mu$m) minimise encapsulation, and thus can both record single neurons for many months and precisely stimulate small groups of neurons. However, such small electrodes are deliecate, and their high impedance requires stimulation voltages that exceed the water hydrolysis point.

We have previously developed an electrode design in which groups of thin electrodes support each other during insertion and then splay in the brain. Here we describe the splaying properties of these electrode arrays. We present preliminary results showing that these electrodes remain capable of recording

individual spikes for a year after implantatiion, and that the spatial scale of the splaying is sufficient to allow the steering of current between the electrodes. We show a proof of concept of two consequences of current steering: it can produce neural responses while keeping stimulation voltages below safety limits, and it permits some control over the shape of the response.

1 Introduction

Direct control of the brain—the ability to sense and modify its dynamics in real time—is a longstanding goal in neuroscience, engineering, and medicine. Sensing has been achieved on a variety of spatial and temporal scales in humans and non-humans, using fMRI, scalp electrode hats, trans-cranial magnetic stimulation, optigenetics, and with surgically implanted electrodes, both on the surface of the cortex and implanted into deep brain areas. The gold standard for spatial and temporal resolution is patch clamping, which can record individual neurons, but is at present infeasible for chronic implants in behaving animals. Small extracellular electrodes can potentially still provide high spatial and temporal resolution, recording individual neurons and stimulating over regions on the scale of a single dendritic tree. Increasing the channel count of these electrodes allows recording signals from different locations simultaneously, as well as greater control over stimulation. Increasing the size of the electrodes makes them more robust and more capable of safely injecting enough current to modify neural dynamics, but comes at the expense of spatial resolution and chronic recording capability. We propose that a multichannel electrode arrays consisting of thin carbon fibres, combined with appropriate current steering, can achieve fine spatial resolution, biological compatibility, safe stimulation, and produce a variety of different neural dynamics.

Much of the work in current steering in the brain is due to interest in deep brain stimulation (DBS). Despite the lack of understanding of the precise mechanisms of DBS, it has been successfully used to treat various movement disorders (especially those associated with Parkinson's disease), epilepsy, Alzheimer's, chronic pain, cluster headache, depression, OCD, addictive behaviours, anorexia, and others [1]. DBS electrodes usually consist of single rods 1.2–1.6 mm in diameter with 4–32 contacts.

Larger electrodes cause more damage both during and after surgery—over the course of weeks and months, glia gradually encapsulate intruding electrodes, rendering them less effective over time. For example, [2] notes a 500-μm encapsulation layer for the $\sim$ 1.3-mm electrodes common in DBS. This encapsulation results in ever-increasing stimulation thresholds, rendering the electrodes unable to record as effectively [3–6].

Even before glial encapsulation, large electrodes lack sufficient spatial resolution to record or stimulate near the single-neuron spatial scale, and instead can sense and modify only local field potentials. At this spatial scale, most current-steering methods use computational models of brain tissue to predict steering configurations that preferentially target the intended area, or make up for errors in electrode placement during surgery [7]. One approach [2, 8] builds a model of the tissue of interest using magnetic resonance imaging (MRI) and diffusion tensor imaging (DTI) [9, 10]. This produces data with voxels of roughly 2 mm^3. They then use finite element analysis to design current-steering patterns to target the desired target. The accuracy of this and related approaches is appropriate given the size of DBS electrodes; however, the techniques will not provide sufficient accuracy to take advantage of the control available with small electrodes.

Lots more references might be added here, all of which have spatial resolution on this order and a variety of temporal resolutions; choose ≈3 or just cite a review?

Do we care? Remove this paragraph?

There has also been interest in current steering outside the brain. For example, [11] describes an algorithm for clinician-assisted hillclimbing search for effective stimulation in multielectrode arrays in the spinal cord.

An important example of current steering outside the brain but in a densely connected network uses 64-channel electrode arrays, with electrode as closely packed as 30 μm, to stimulate macaque retina *in vitro* [12]. They stimulated the retina using single electrodes or combinations of three electrodes with charge-balanced pulses, and found that retinal response could be predicted with a piecewise linear model of the steered current. The connectivity of retinal cells differs from that in most other brain regions, but we feel that this experiment nonetheless hints at the potential of neuron-scale current steering.

Most DBS systems deliver some fixed stimulation pattern continuously. Recently, interest in using biological feedback to tune medical devices has grown. Due to the size of the electrodes, for feedback control most systems rely on large-spatial-scale metrics such as local field potentials (LFP) [13] and other macroscopic measures of

Great review: [15]

outcome such as surface electromyography and accelerations [**?**, 14]. The addition of feedback from a second electrode in a related brain region is effective in ameliorating Parkinsonian symptoms in monkeys [16], in which the use of tungsten microelectrodes demonstrated the effectiveness of feedback that responds to individual spikes rather than just LFPs.

Insertion damage, glial encapsulation over time, and poor spatial scale of large electrodes are all mitigated by electrodes < 10 μm, but these present two difficulties: they are too fragile to insert easily, and during stimulation, their small surface area requires dangerously high voltage in order to deliver sufficient current to induce response.

The electrode array of [17] overcomes the structural fragility of thin electrodes by using multiple (in our case, 16) shanks each of which, at 7 μm, is small enough to avoid adverse tissue reactions. They bundle together to support each other structurally during implantation, and separate and splay in the brain, giving randomly distributed sites for recording and stimulation. Here we quantify that splay.

Why current-controlled? E.g. [8]?

In a current-controlled stimulating electrode, the voltage required to induce neural activity goes up as the impedance increases and charge injection capacity decreases. Neural damage is likely to occur when voltage exceeds the hydrolysis point for water (around 1.2 V). This is not a problem for large DBS electrodes, whose surface area tends to be ample and which are in any case encapsulated by glia, but it creates a problem for our small electrodes (area per shank is around 250 μm^2): their impedance is high and their charge delivery capacity is poor, leading to high voltage requirements for stimulation.

We address the voltage problem in two ways. First, we confirm that electroplating the electrodes in iridium oxide, as suggested by [18], leads to roughly a tenfold improvement in both impedance and charge injection capacity. Second, we introduce a novel current-steering technique, and provide preliminary evidence that appropriate choice of current-steering configuration can be used to reduce stimulation voltage.

Confirm improvement in charge delivery. Yarden has numbers of gold → IrOx, but do we have carbon → IrOx anywhere more systematic than my own data? But more than that, since we only did this with one chronic electrode (and the short-term birds), is it even worth listing here? Or should I just mention it in Methods?

Due to their size, the multichannel, spatially distributed, micron-scale arrays introduced in [17] allow long-term single-unit recordings, enabling new experiments investigating how the brain changes on long timescales. Here we provide preliminary evidence showing:

- How often the electrodes splay correctly in the brain, and the spatial scale of that splay.
- That the electrodes can record activity in single units a year after surgery.
- That the electrodes can be used to stimulate the brain.
- That the spatial scale of splay is sufficient to allow effective current steering.
- That current steering can be used to reduce injected voltage, thus keeping neurons safe while still delivering clinically significant results.
- That current-steered control of stimulation inputs allows fine-grained control over small groups of neurons, potentially permitting a wide variety of optimisations, such as controlling the brain to some set of desired responses.

We were able to build only a limited supply of the electrode arrays, and thus provide chronic stimulation data from a very small number of birds. This is a serious limitation of the study, and thus our results should be regarded as preliminary. However, we believe that even as they stand they will nonetheless be of interest to the community, suggesting capabilities that have not heretofore been available.

2 Materials and Methods

2.1 Electrode construction

Electrode arrays were constructed as described in [17].

2.1.1 Charge injection

The charge transfer capacity of one of the electrode arrays (16 shanks) used for stimulating in Area X was enhanced by electrodeposited iridium oxide. This effects an improvement of roughly an order of magnitude: impedances went from around 2 MΩ to 200 kΩ, and for a given current, the required voltage was much lower. We also experimented with PEDOT, which has excellent charge-injection properties, but we found it to have durability issues. A detailed analysis is outside the scope of this work See [18] for a review of charge transfer physics.

FIXME

All I know about this is hearsay.

2.2 Bird surgery description

2.2.1 Animals and Perfusions

At the end of the experiment, the birds were given an overdose of pentobarbital and perfused with 0.1M phosphate buffer followed by 4% paraformaldehyde in 0.1 M PB. Brain with skull were removed. The electrodes were secured on the skull and brain. 2–4 holes were made on the skull to facilitate the solutions to get in. Following an overnight postfix in 4% paraformaldehyde, brain with skull was treated overnight in 15% and 30% sucrose in 0.1M PB at 4°C. Brain slices with the electrodes were collected. The tissue samples were sectioned towarding to the tips of the implanted elctrodes at 50–100μm by a cryostat (CM 3050 S, Leica). The tissue samples were stored in −20°C until immunohistochemistry was processed.

Which?

2.2.2 Fluorescent Immunohistochemistry of NeuN, MBP and DAPI

Sections of the brain were used for immunohistochemical staining of Neun and DAPI. Non protein binding was blocked with 5% normal donkey serum. The primary antibody against neuronal nuclei was a mouse anti-NeuN antibody (1:500, MAB377, A60, Chemicon) and the primary antibody against myelin was a rabbit Anti-Myelin Basic Protein / MBP Antibody (1:500, LS-C312288, LifeSpan BioSciences, Inc). Following primary antibodies incubation for overnight at 4°C, Alexa Fluor® 488 AffiniPure Donkey Anti-Mouse IgG (H+L) (1:500, 715-545-150, Jackson ImmunoResearch Laboratories) and Rhodamine (TRITC) AffiniPure Donkey Anti-Rabbit IgG (H+L) (1:500,711-025-152, Jackson ImmunoResearch Laboratories) added. The sections were coated with mounting medium containing 4',6-diamidino-2-phenylindole (DAPI, VECTASHIELD). The sections of brain were visualized and the images were captured using a FV10i confocal microscopy(Olympus) and Olympus FV10i software.

2.2.3 Surgery information

All procedures were approved by the Institutional Animal Care and Use Committee of Boston University (protocol number 14-029). Zebra finches (n = 15: 13 for acute splay histology, 2 for chronic HVC and Area X recordings) (>120 days post-hatch) were

Include the third?

anesthetized with 4.0% isoflurane and maintained at 1–2% isoflurane during the aseptic surgical procedure. The analgesic Meloxicam (4mg/kg) was injected intramuscularly into the breast at the start of the procedure and the animal was placed into a stereotaxic instrument. Feathers were removed from the scalp and a Betadyne solution applied. Bupivicane (4mg/kg) was then injected subcutaneously into the scalp before an incision was made along the AP axis.

The same surgical procedure was followed for the acute and chronic recording in Area X and HVC [17]. The skull over area X was localized using stereotactic coordinates (20° head angle; 5.8 mm AP, 1.5 mm ML, 2.8 mm DV) and the skull over HVC was localized using stereotactic coordinates (30° head angle; 0.7 mm AP, 2.3 mm ML, 0.4-0.7 mm DV), and the the outer bone leaflet removed at the location of area X and HVC with a dental drill. The lower bone leaflet was carefully removed with an opthalamic scalpel, similar to implant procedures for recording with microdrives [19], exposing a hole of $\sim 150\mu$m diameter. A minimal durotomy was performed using a dura pick (typical durotomy was less than 50 microns.). A 16-channel carbon-fibre array [17] was mounted on a digital manipulator attached to the stereotax and slowly lowered through the durotomy. During insertion into the brain, the carbon fibres would occasionally begin to visibly splay. After lowering the array to the appropriate depth, the position in the song nucleus HVC was verified using antidromic stimulation from another 16-channel array implanted in downstream Area X [17, 20]. After verifying the position of the array, the craniotomy was covered with the silicone elastomer Kwik-Sil (World Precision Instruments), and the array was glued into place using light-bonded acrylic (Flow-It ALC, Pentron) along the entire length of the electrode shank, such that no portion of the carbon fibre bundle was left exposed or loose. A $\sim 150\mu$m hole was made on the skull of cerebellum and both arrays' grounding wires were secured in cerebellum using light-bonded acrylic.

2.3 Splay histology

Electrode bundles were implanted into birds, all to a depth of roughly 3 mm. Most of these were "dummy" uncoated and blunt-cut rather than fire-sharpened as in [17], with 10–16 channels (fibres). The birds were killed, and their brains sectioned roughly

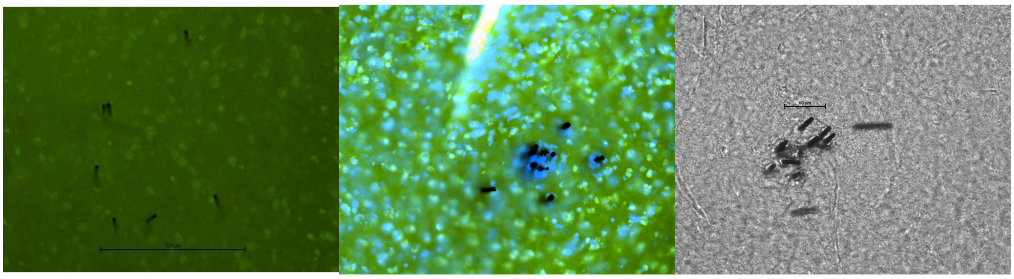

Figure 1. Splay types, left to right: examples of full splay, partial splay, and clumped. In all images, black circles are electrode shafts; in many cases the slicing plane is not quite orthogonal to the electrodes, yielding oblong images. In the bright-field image on the right, three of the electrode slices were pulled out of the tissue during slicing, and appear to lie flat on the slide. Since their original locations cannot be determined, we have ignored them.

Jun & Sanne: what slice thickness?

perpendicularly to the electrodes, with a slice thickness of 50 μm.

Sanne: check exclusion criteria.

The following criteria were used to exclude observations:

- Individual shafts were excluded if they were lying flat on the surface of the tissue (visible as side-on cylinders).
- Bundles were excluded if they were implanted in fibres of passage.

Clustering was done by hand. The set of distances between electrodes was computed by measuring the distance between each electrode and its nearest neighbour.

I'm about a day from finishing software to do all-to-all comparison. For the draft (and possibly first submission, if time is tight) this suffices.

Bundles were clustered as follows:

Splayed: All electrodes were more than 10 μm from each other, or at most one pair was closer.

Why 10 μm?

How many?

Partial: Some electrodes were more than 10 μm from each other.

All-to-all, or nearest-neighbour?

Clumped: All electrodes were within 10 μm of each other.

Would it make sense to automatically cluster the splay data? Or to change the criteria? I can think of some changes...

Examples of these three categories are shown in Fig. 1.

2.4 Recording

For electrophysiology (recording and stimulation), birds were anesthatised with 1.5% isoflurane, 98.5% oxygen, at 0.5 liters/minute.

Recording of spontaneous activity in Area X was with an Intan RHD2000 amplifier at 20 kHz, with a high-pass filter at 200 Hz. Recordings were broken down into data files 1 minute long. Any data file with any sample whose absolute value was $> 500\mu$V was assumed to have excessive recording noise, and was discarded.

2.5 Stimulation: Zebra finch antidromic HVC ← X

Electrical stimulation saturates the brain, including at the site of the recording electrode, for some time post-stimulation. Artifacts were visible in the recording traces for 1–3 ms post-stimulus. Responses to stimulation can be detected outside of that saturation window. A common technique for locating HVC in the zebra finch involves implanting a stimulating electrode in Area X and looking for a an antidromic response, which is visible in HVC and not in the surrounding tissue [20, 21]. Since the two brain areas are separated by about 5 mm, this response occurs 3–8 ms after stimulation, which gives the recording amplifier time to settle before measuring the response.

Tim: citation for 3–8 ms?

But why antidromic?

For discussion of the stimulation paradigm, we will use the following definitions:

Channel: Our electrodes have 16 channels, each of which is an individual carbon fibre connected to its own amplifier.

Pulse: A biphasic charge-balanced square wave of current. Each phase is 200 μs long, and there is no interpulse interval.

Current steering: Delivering pulses, usually of opposite signs, to two or more electrodes in order to control the geometry of current flow through the tissue.

Current-steering configuration (CSC): The configuration defining which channels receive the positive half of their biphasic pulse first, or vice versa.

Pulse train: A sequence of n (usually 10) identical current-steered stimuli delivered to all active channels, usually at 25 Hz. This is slow enough that pulses do not interfere with each other, and is used to measure the reliability of the response.

Threshold scan: A series of pulse trains, each of which has the same CSC but a different current, designed to find the minimum current for this CSC that will induce an antidromic response in HVC. The algorithm is described below.

Voltage scan: The Plexon hardware can deliver a current-controlled pulse to each of 16 channels independently and simultaneously, but only allows monitoring of the voltage delivered on one channel at a time. A voltage scan involves sending the same pulse train once per active electrode, monitoring a different one each time.

The stimulation and recording electrodes use separate electrical returns, consisting of silver wire in contact with the skull. Some CSCs balance current delivery between the electrodes, whereas others do not, and in the latter case excess current flows through the common return.

We used a Plexon stimulator to control stimulation in Area X, and recorded from HVC using a Tucker-Davis Technologies (TDT) RZ5 amplifier or an Intan RZ2000. The Plexon self-monitoring channels were recorded on a National Instruments (NI) PCI-6251 data acquisition card using the session-based interface of Matlab (various versions from 2014a through 2015b) on Windows 8.1.

Model #? Also depending on which recording to show in Fig. 2

Custom MATLAB software controls the experiment, initiating spike train delivery and response monitoring. The Plexon's self-monitoring channels are recorded by the NI card, and the neural response in HVC is recorded by the TDT. In order to guarantee precise temporal alignment between stimulus delivery and response measurement, all hardware is triggered by a TTL pulse from the NI card when it begins its acquisition cycle. The Plexon begins stimulating upon receipt of that TTL pulse, and the TDT begins recording at 24.414 kHz (the device's native frequency) on the same signal. Whenever the Plexon is actively delivering current (i.e. during each pulse within the train) it sends out its own TTL pulse: this signal is recorded by the TDT along with the HVC electrode voltages. Thus the data alignment precision is controlled by the sampling rate of the TDT (41 μs).

Programming each of the stimulator's 16 channels for one pulse train and running the programme (10 pulses at 25 Hz) requires a little over 2 seconds. A threshold scan requires, on average, around 15 pulse trains, and so generally takes a bit more than 30 seconds. Likewise, a voltage scan requires delivering one pulse train per active electrode, for a total of about 30 seconds.

This timing is after I did some speedup hacking, but the experiments presented in this paper were pre-speedup (about half as fast). Does it matter?

2.5.1 Response detection

HVC projects into Area X (and into RA, which we do not discuss here). When Area X is stimulated, an antidromic response may be observed both in HVC_X projection neurons and in HVC interneurons. The antidromic response occurs roughly 3–8 ms after the stimulation pulse, and is highly stereotyped: [22] reports that the variability in the timing of the antidromic response in HVC_X projection neurons is under 50 μs, while that of HVC intraneurons is above 500 μs.

Fig. 2 shows an example of a pronounced HVC response to stimulation in Area X. We detected this response in two different ways, one during experiment runtime and one in postprocessing analysis:

During runtime (threshold and voltage scans), we measured the cross-correlation between the recorded response for each pulse in a train and each other with a maximum lag of 100 μs, which provides a robust way of separating neural response from noise. Because the HVC amplifier's (Intan's or TDT's) response to the transient stimulation pulse in Area X can persist into the time of interest (3–8 ms), each response is first de-trended using a maximum-likelihood fit over the region 2–25 ms using an eigth order Fourier Series, which removes post-stimulation decay while leaving spike-sized signals intact. We found that this strongly biased smoothing technique more cleanly removes the large stimulation artifact than the conventional approach of bandpass-filtering the signal. The cross-correlation threshold above which a response is identified is chosen by visual inspection.

Filtering would probably work better with the TDT than with the Intan...

A further, independent voltage-threshold analysys was performed on the data offline. For each train of n pulses, we labeled peaks greater than 5 standard deviations from the RMS noise of a nearby (within 20 ms) non-stimulated recording on the same electrode. For each of the n stimuli in the pulse train, all peaks' delays post-stimulus were compared to those from the other $n-1$ responses, and any peak whose delay was within 100 μs of another peak was considered a response to the stimulus. The probability of a response at this current was then the maximum number of aligned peaks divided by the number n of pulses in the train. Given the set of points $\Pr(\text{response} \mid \text{maximum electrode voltage})$, we then fit a sigmoid $0.5(1+\tanh(\lambda(x-\mu)))$ to this curve, and take the midpoint μ as the voltage required

to induce a response with probability 50%.

Details or citation? Possibly [3], although they don't really discuss this so much.

As the bird ages, the implant bonding site is slowly pushed away from the skull. For shallow installations such as HVC (depth $\approx 200\mu m$, the quality of the HVC recordings diminishes as electrodes are forced out of contact with the brain. This makes it more and more difficult over time to measure the antidromic response. The above cross-correlation technique for response detection is more sensitive than the method typically used during acute or short-term response measurements, in which a pronounced spike is often clearly visible and is identified by eye on an oscilloscope. We are confident that we are measuring an antidromic response because it is on the correct timescale both in delay post-stimulus and in consistency, appears near the expected stimulation threshold, and has the expected shape.

Cite papers giving timing and stimulation threshold.

2.5.2 Threshold scan

What stimulation parameters are required in order to reliably elicit an antidromic response to stimulation in Area X? How can this threshold be found quickly, while minimising the risk of exceeding safe stimulation voltages? How can this process be made robust to noise?

How can we establish how much robustness to noise is required?

After choosing a CSC, we begin stimulating at a current that is known to be below threshold. While no response is seen, the current is increased gradually by a small factor $\alpha = 1.1$ until either a response is detected or the voltage or current limit is exceeded. In the latter case, a lack of response is reported, and we move on to the next CSC. If a response is found, then the step size is decreased towards unity ($\alpha \leftarrow \alpha^{2/3}$) and we reduce the current until the response disappears. This process is repeated until the step size drops below a limit ($\alpha < 1.02$), and the threshold is taken as the last parameter set that induced a response.

While a larger step size would result in a faster search, and a binary search would in addition be easier to describe, this ad-hoc approach samples near the current of interest while making it unlikely that we will stimulate with a current that significantly exceeds the minimum required for a response, and thus minimises the possibility of injuring the bird.

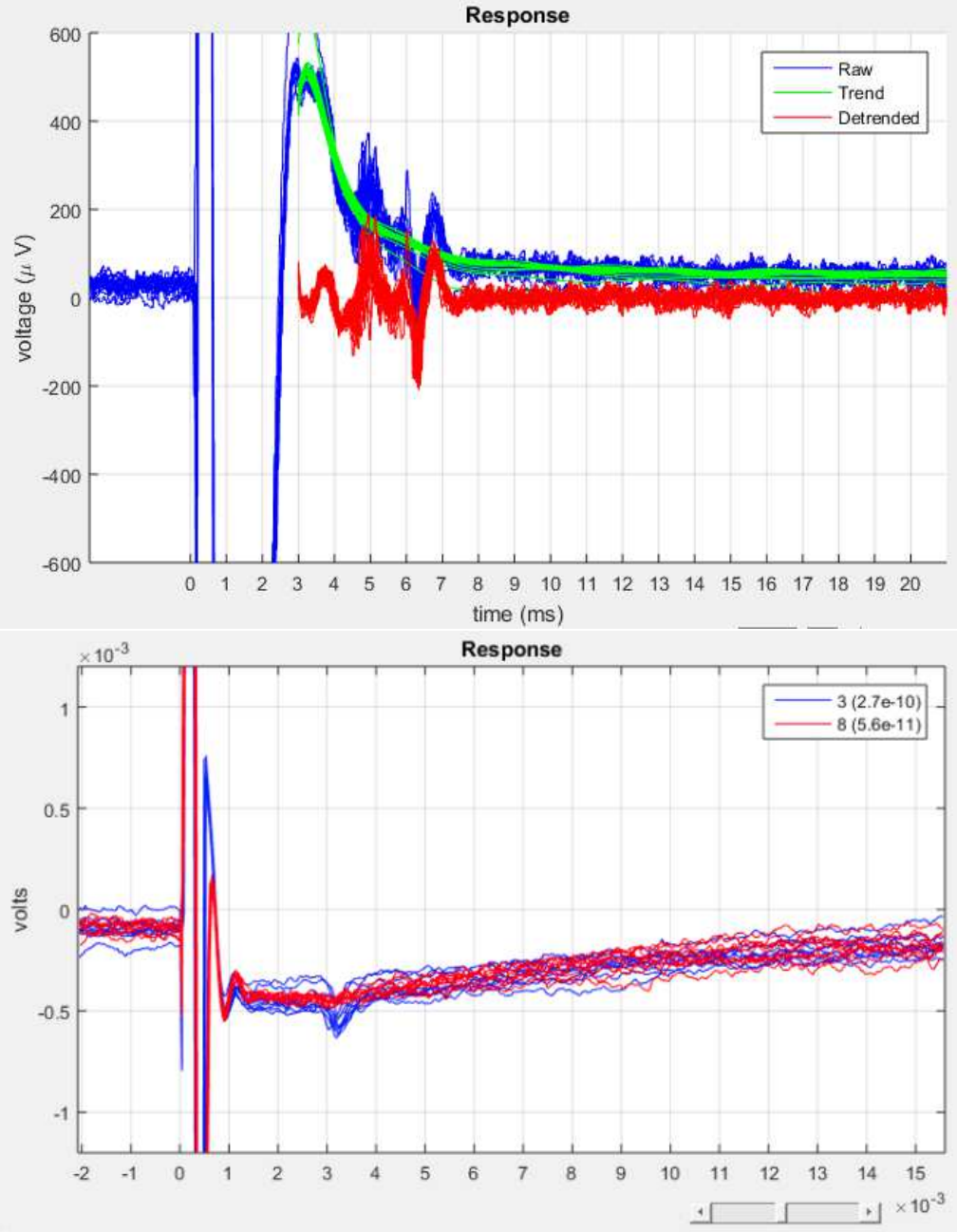

Figure 2. An example of a strong response in HVC. **Top:** The horizontal axis is time in milliseconds relative to the onset of a stimulation pulse. Here, the stimulation is a 400-μs biphasic pulse of 3 μA, in which voltage peaked at 1.6 V. Stimulation was repeated 20 times at 25 Hz, with each response aligned to its respective pulse to within 41 μs. Various response activity can be seen, but the most pronounced is at 6.2 ms post-onset. **Bottom:** a different bird, with a much weaker signal, but recorded on TDT. 200 μs, 6.94 μA, 1.2 V peak. *Use the top figure? It only shows one channel, and it's recorded on the Intan, which I was using while the HVC signals were still pretty. That means a lot worse amplifier settling, so it's not the best image, but the response is much cleaner than later ones made with the TDT.*

# Good electrodes	Inter-electrode distance (μm) Mean	StdDev	Max
3	5.0	0	20.0
10	6.0	2.1	52.9
16	6.3	6.3	48.3
4	7.5	5.0	35.8
6	16.7	18.9	44.8
9	7.7	5.5	107
14	12.8	12.1	15.2
8	14.7	17.8	108
15	15.1	10.2	163
15	19.3	19.1	128
5	22.0	27.7	103
9	28.2	35.8	148
11	31.8	28.1	103
8	35.9	30.6	228
13	76.5	152	167
5	51.4	28.1	51.5
3	20.0	0	123
6	73.5	35.5	128
8	38.5	35.2	142
9	47.4	31.5	208
5	126	63.5	214
16	62.0	58.9	829

Table 1. Raw data. Each row shows the statistics from one electrode array. "Good" electrodes is the the number of carbon fibre electrodes in each bundle that appeared to still be firmly fixed in the neural tissue after slicing.

2.5.3 Voltage scan

Once the minimum current required in order to achieve a response is identified, we perform a voltage scan at that current, in order to measure the peak voltage delivered to each electrode.

3 Results

3.1 Splay histology

After exclusion, 22 arrays, implanted into 13 different birds, each yielded at least 3 measurable electrodes. See Table 1 for the raw data and Fig. 3 for visualisations thereof.

Perhaps take out the table and just use the graphs?

Fig. 4 shows some examples of the damage done to the brain in the vicinity of the electrodes. Visual inspection shows little damage in the vicinity of single electrodes, and slightly more in clumped electrode groups. Visual inspection can give some

An image of "typical" damage done by "micro"electrodes would be nice, but it's hard to show what's typical of the ~~competition~~ prior work with any credibility. Letting people compare vs. their own experiences is the best, but not everyone (e.g. me) will know what's typical.

I have data on how long post-implant the birds lived before these data were taken, which needs to come along with this figure or somewhere.

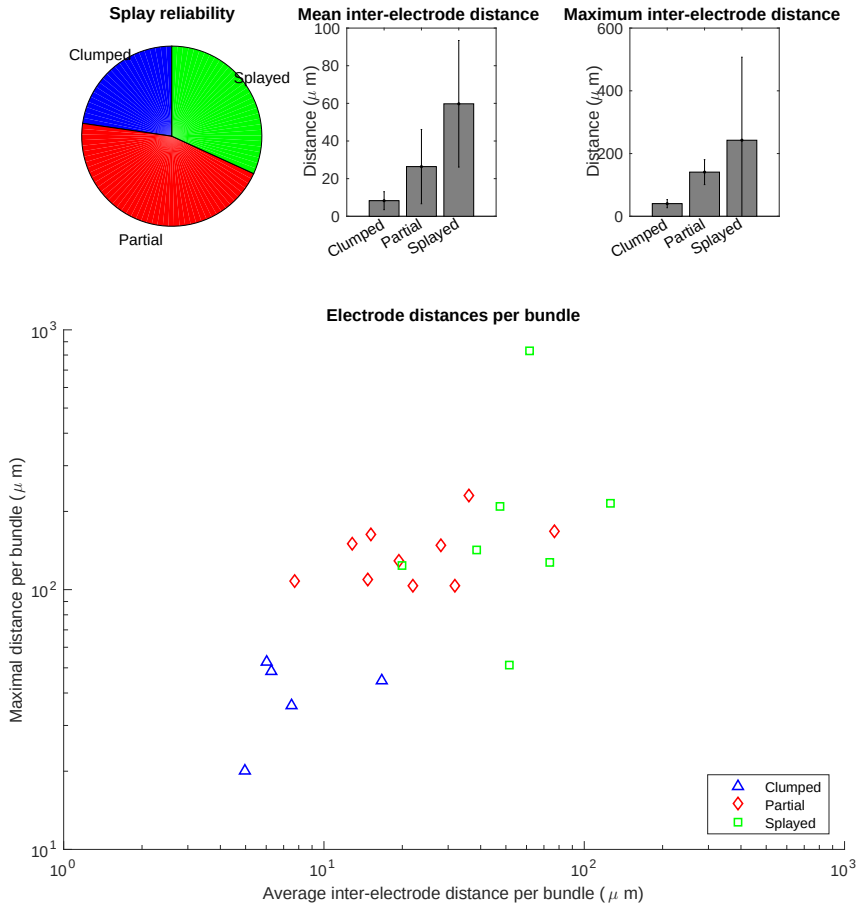

Figure 3. Splay histology data from Table 1.

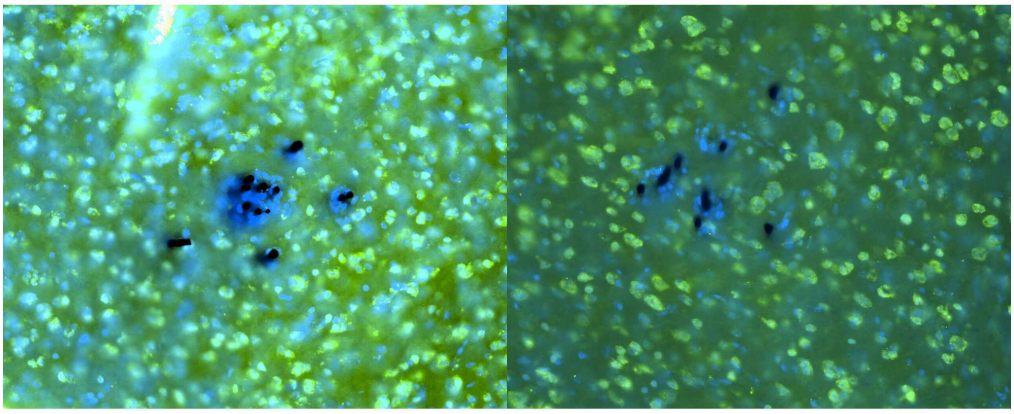

Figure 4. Typical damage. Neural nuclei are shown in green (stained with NeuN) and all cells in blue (DAPI). The presence of non-neural cells indicates damage, and is notable in the vicinity of the largest non-splayed electrode bundle, and nearly absent around individual electrodes.

indication of the damage done to the brain and the likelihood of achieving good electrical contact with neurons, but we are more interested in the ability to interact with the brain (see Section 3.2).

3.2 Chronic recording

3.2.1 Impedances

3.2.2 HVC

Long-term recording in HVC is difficult due to skull regrowth interfering with electrodes implanted only a few hundred microns from the surface: after 10 months, we had difficulty picking up antidromic response in our two remaining birds, and while the techniques described in Sec. 2.5.1 were more sensitive and robust than detection by eye, eventually the signal-to-noise ratio became too low for them as well.

3.2.3 Area X

More telling of the potential of these electrodes to detect spikes is the recording of spontaneous activity in Area X, which was still easily seen in several channels after a year. Fig. 5 shows recordings a year after implantation for the most stable electrodes of the 16.

I don't have recording-only data from early on.

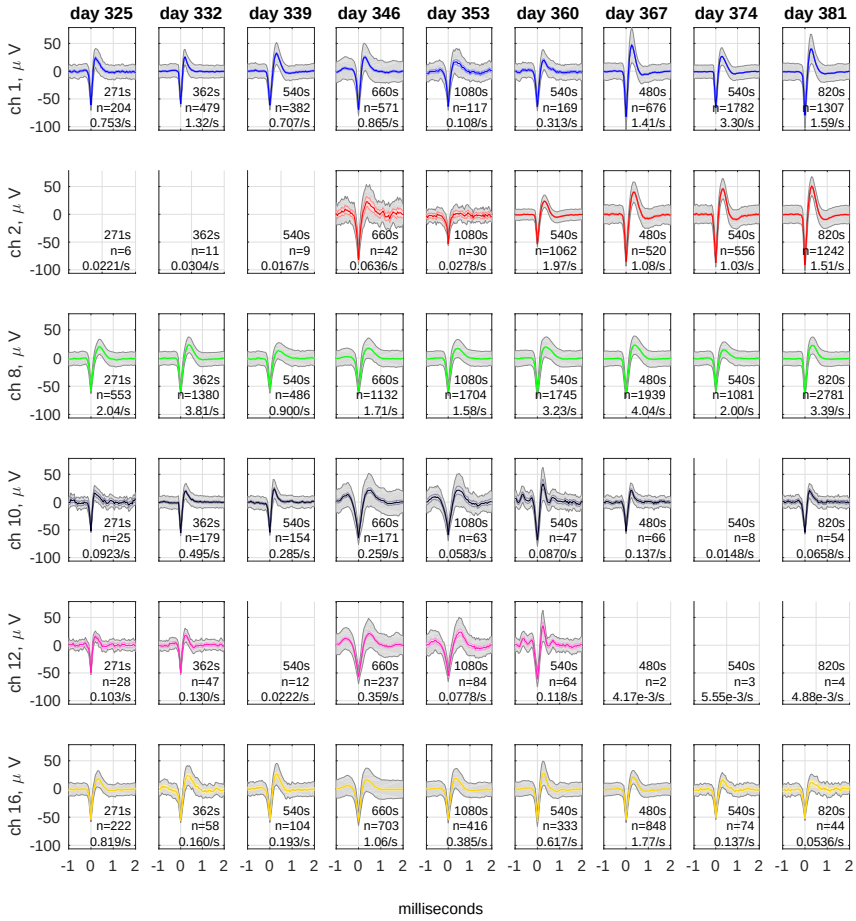

Figure 5. *FIXME Here I show 6 electrodes. 3 are beautiful, and 3 fade in and out. What's the best way to present this? Should I omit graphs with fewer than 20 spikes as I've done here Or show their messy squiggles?* Some of the electrodes in Area X record spontaneous spikes a year after implantation. Column titles show the day post-surgery and the number of seconds of recorded data. Each row is one electrode (shown here: the three most stable channels and three that showed some variability). Legends show the number of seconds of the recording, the number of spikes, and mean spike rate. The grey shaded region is standard deviation, and the coloured shaded region is the 95% confidence interval for the mean.

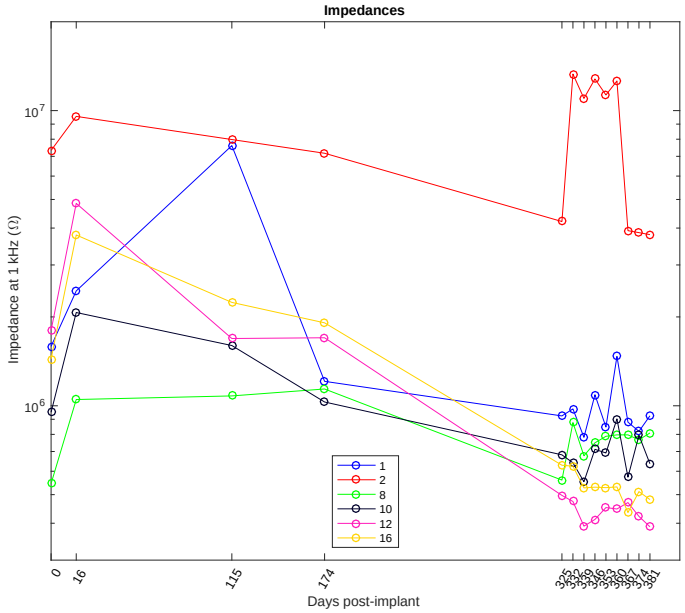

Figure 6. Impedances for the electrodes shown in Fig. 5. Most good electrodes were in the range 400 kΩ–1MΩ for the recordings shown in that figure.

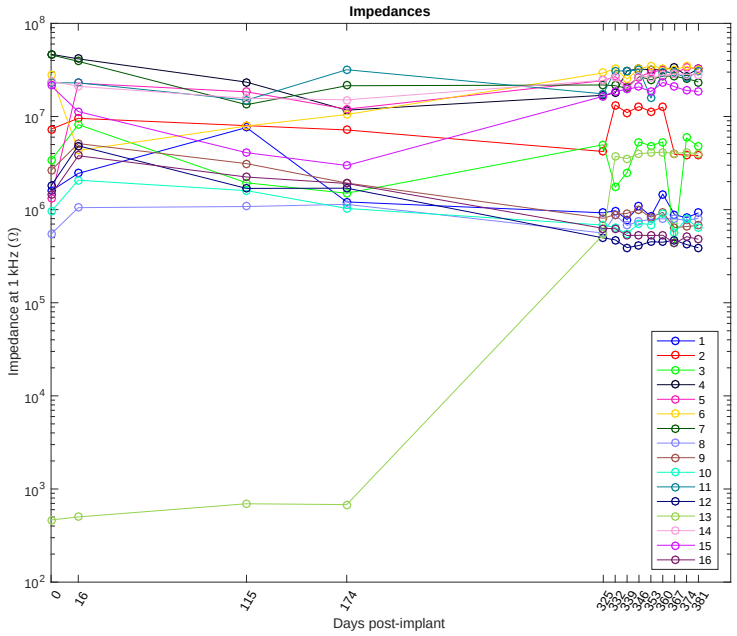

Figure 7. *Full version of Fig. 6. I think I like that one better, but this could be more useful despite (or because of) showing a bunch of bad electrodes...*

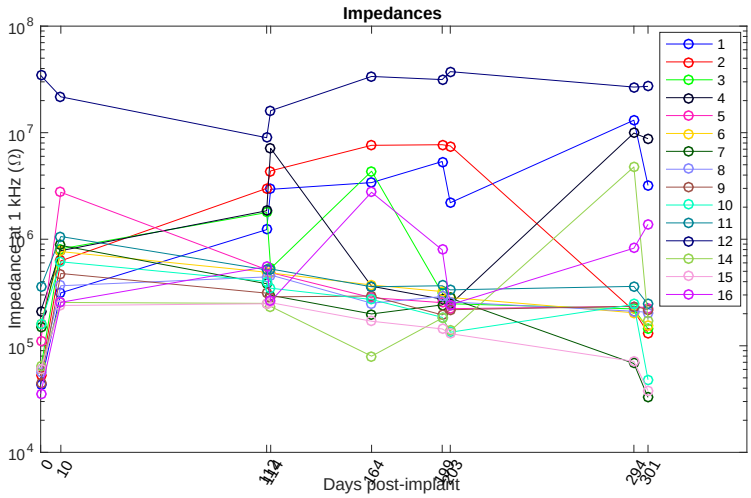

Figure 8. Electrode impedances over time on another bird. This Area X array was treated with iridium oxide. *This plot probably requires a bunch more explanation. Notably: why the big jumps? Need to check on stimulation, but hard to generalise with so little data...*

3.3 Stimulation

3.3.1 Minimising stimulation voltage

Explain why this number. Why only one bird?

Some CSCs were better at triggering an antidromic response than others. From the 2^{11} possible CSCs we chose 32 (30 randomly, and the two that treated all electrodes identically). For each CSC, we performed a threshold scan to find the minimum current needed to trigger a response. When this current was found, we performed a voltage scan to find the maximum potential on any electrode. We tested each CSC five times on an anesthetised bird. Results are shown in Fig. 9. The best CSCs resulted in a maximum voltage of around 1 V, while the worst were over 2.5 V. Perhaps surprisingly, the CSCs that sent identical pulses to all 11 electrodes were among the worst performers, with our simple search revealing CSCs that kept voltages far lower.

The maximum-likelihood fits to the voltage sweep data (green errorbars in Fig. 9) consistently yield slighly higher threshold voltages than those measured using the search. This is because whereas the maximum-likelihood fit computes the voltage required in order to obtain a response with 50% probability, the threshold search, which guided data acquisition in realtime, looks for any significant correlation between the responses in each spike train, which is detectable well before the stimulation

achieves a 50% response rate.

3.3.2 Controlling the antidromic response

4 Discussion

4.1 Steering

[12] showed good capacity to control stimulation by steering current between electrodes in monkey retina, allowing targeting of neurons on a smaller scale than the electrode spacing. The demonstration of fine control is compelling, but whether or not the locally linear predictive response model that they found effective in retina would be extensible to regions with greater lateral connectivity is unknown.

[23] showed that injecting current into tissue causes neurons whose axons are very close to the stimulation site to fire, rather than neurons whose bodies are at greater distances. As a result, the set of neurons that respond to a stimulation pulse is highly sensitive to electrode location, but has spatial extent similar to that of the neuron's dendritic tree. Furthermore, they showed that neurons stimulated in this manner seldom stimulate downstream neurons synaptically.

Splaying electrode arrays with learning stimulation software may be able to exploit these properties. First consider each of the n electrodes in our array separately. n sites stimulated at a given current yields up to n different random sets of k_n neurons that will fire, and increasing the current changes the size of k. There may exist multiple downstream neurons y such that directly-stimulatable neurons from several of our n sets synapse onto y. This creates a search problem: how to stimulate the n sets in a way that reliably stimulates y enough to cause it to spike? This requires search over current delivered to each group in n in order to control which neurons are recruited, and timing of stimulation delivery to each group in n, so that appropriate downstream neurons are reliably triggered. Different values of current and timing delivered into the n groups may trigger different downstream neurons, so one possible search problem is finding as many different downstream neurons as possible.

Furthermore, it seems likely that directly-stimulatable neurons may synapse onto others that are directly-stimulatable, once or r times removed. This suggests a more

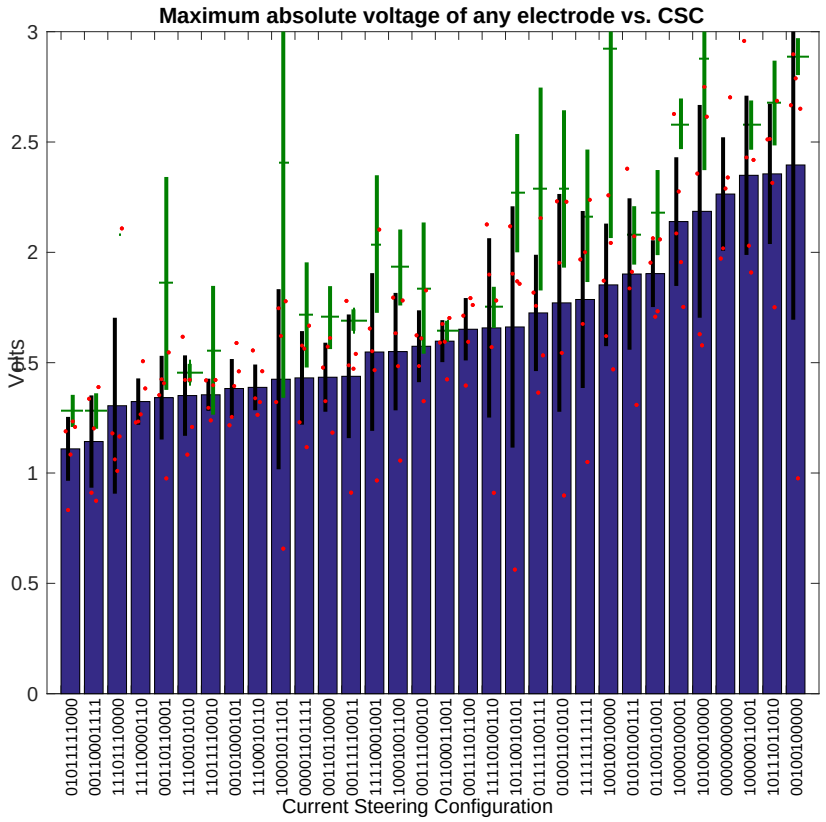

Figure 9. The peak Area X stimulation voltage required in order to achieve biologically effective levels of stimulation in HVC varies with different current-steering configurations. Here are 32 different configurations, over 5 trials each, taken 214 days post-surgery. The X axis lists the configuration (each of the 11 active electrodes delivers a positive-first "0" or negative-first "1" current-controlled pulse). The Y axis shows the maximum voltage across any electrode for the given CSC at the lowest current that evoked a reliable response. Blue bars are the mean voltage discovered using the online threshold scan technique described in Methods, red dots show the voltage result for each trial, and error bars are 95% confidence intervals (n=5). Green bars show the voltage required to induce 50% probability of response using a the maximum-likelihood analysis described in Methods, also as 95% confidence intervals (when the confidence lines would have spanned the whole range of the graph, they have been omitted for clarity), and with crossbar marker at the mean, with marker width chosen to give an approximate sense of confidence. *FIXME Cosmetic stuff: xlabel/ylabel collisions, expand Y axis, maybe angle the CSCs, and why a bar graph?*

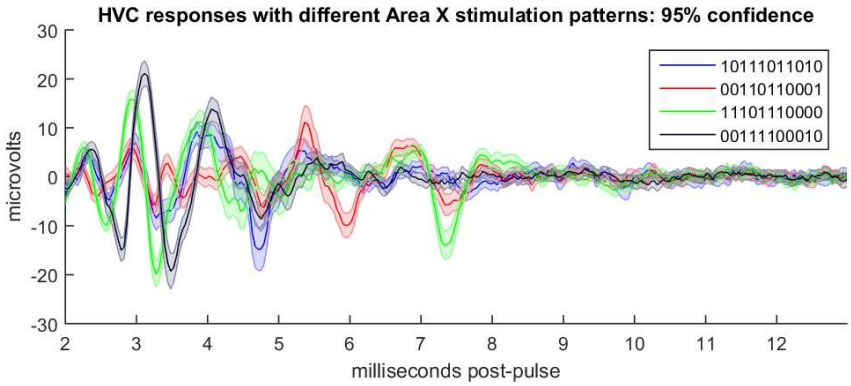

Figure 10. Different CSCs delivered to Area X can induce different responses antidromically in HVC. Here are four of the most distinct responses to four of the 32 CSCs shown in Fig. 9. Shading is 95% confidence, n=198.

general objective for the search, in which different timings for stimulating the n sets may trigger different network-scale dynamics. ([12] proposes a related mechanism in the context of current steering in retina). This enlarges the space of inducible dynamics considerably, and suggests the possibility of inducing Hebbian learning.

Whereas Histed used single electrodes, we use miltichannel arrays. Rather than a 16-channel array providing $n = 16$ groups of neurons, different current-steering configurations may lead to a much higher value of n. For such an electrode there are 2^{16} current-steering configurations even without manipulating current pulse magnitude or timing, and with those additions the search space is nearly infinite.

4.2 Ongoing Learning

DBS treatments depend on finding the most effective stimulation patterns given electrode placement and patient response. The best clinical outcomes require about 20 hours of hand-tuning, involving multiple patient visits to a clinic.

Now where did I read this... CITATION NEEDED?

This has nothing to do with our paper. Learning is not addressed here. But I could mention it as a possibility. Should I? Or leave it out?

4.3 Power

Another limitation of DBS systems is power use: even when the system only activates in response to need (on-demand DBS), the currents required in order to achieve good clinical outcome drain power. Small electrodes that drastically reduce scarring allow stimulation currents several orders of magnitude lower than state-of-the-art systems, and even if current steering does not allow realtime therapy optimisation, it appears to

allow further optimisation of power usage.

References

1. Udupa K, Chen R. The mechanisms of action of deep brain stimulation and ideas for the future development. Progress in Neurobiology. 2015;133:27–49. Available from: http://www.sciencedirect.com/science/article/pii/S030100821500088X.

2. Butson CR, McIntyre CC. Current steering to control the volume of tissue activated during deep brain stimulation. Brain Stimulation. 2008;1:7–15. Available from: http://www.sciencedirect.com/science/article/pii/S1935861X07000058.

3. Barrese JC, Aceros J, Donoghue JP. Scanning electron microscopy of chronically implanted intracortical microelectrode arrays in non-human primates. J Neural Eng. 2016 April;13(2). Available from: http://www.ncbi.nlm.nih.gov/pmc/articles/PMC4854331/.

4. Biran R TP Martin DC. Neuronal cell loss accompanies the brain tissue response to chronically implanted silicon microelectrode arrays. Experimental Neurology. 2005 September;195(1):115–126. Available from: http://www.ncbi.nlm.nih.gov/pubmed/16045910.

5. VS P, PA T, WM R. Response of brain tissue to chronically implanted neural electrodes. Journal of Neuroscience Methods. 2005 October;148(1):1–18. Available from: http://www.ncbi.nlm.nih.gov/pubmed/16198003.

6. Winslow BD, Christiensen MB, Yang WK, Solzbacher F, Tresco PA. A comparison of the tissue response to chronically implanted Parylene-C-coated and uncoated planar silicon microelectrode arrays in rat cortex. Biomaterials. 2010 December;31(35):9163–9172. Available from: http://www.sciencedirect.com/science/article/pii/S0142961210006873.

7. Holloway KL, Gaede SE, Starr PA, Rosenow JM, Ramakrishnan V, Henderson JM. Frameless stereotaxy using bone fiducial markers for deep brain

stimulation. J Neurosurg. 2005;103(3):404–413. Available from: http://thejns.org/doi/abs/10.3171/jns.2005.103.3.0404.

8. Chaturvedi A, Foutza TJ, McIntyre CC. Current steering to activate targeted neural pathways during deep brain stimulation of the subthalamic region. Brain Stimulation. 2012 July;Available from: http://www.sciencedirect.com/science/article/pii/S1935861X11000672.

9. Tuch DS, Wedeen VJ, Dale AM, George JS, Billiveau JW. Conductivity tensor mapping of the human brain using diffusion tensor MRI. PNAS. 2001 September;98(20):11697–11701. Available from: http://www.pnas.org/content/98/20/11697.full.pdf.

10. Alexander AL, Lee JE, Lazar M, Field AS. Diffusion Tensor Imaging of the Brain. Neurotherapeutics. 2007 July;4(3):316–329. Available from: http://www.ncbi.nlm.nih.gov/pmc/articles/PMC2041910/.

11. King JDH. Method for optimizing search for spinal cord stimulation parameter settings. Google Patents; 2006. US Patent 7,146,223. Available from: https://www.google.com/patents/US7146223.

12. Jepson LH, Hottowy P, Mathieson K, Gunning DE, Dabrowski W, Litke AM, et al. Spatially Patterned Electrical Stimulation to Enhance Resolution of Retinal Prostheses. Journal of Neuroscience. 2014 April;34(14):4871–4881. Available from: http://www.jneurosci.org/content/34/14/4871.full.

13. Priori A, Foffani G, Rossia L, Marceglia S. Adaptive deep brain stimulation (aDBS) controlled by local field potential oscillations. Experimental Neurology. 2013 July;245:77–86. Available from: http://www.sciencedirect.com/science/article/pii/S0014488612003755.

14. Afshar P, Khambhati A, Stanslaski S, Carlson D, Jensen R, Linde D, et al. A translational platform for prototyping closed-loop neuromodulation systems. Frontiers in Neural Circuits. 2012 January;6(112). Available from: http://www.ncbi.nlm.nih.gov/pmc/articles/PMC3551193/.

15. Priori A. Technology for Deep Brain Stimulation at a Gallop. Movement Disorders. 2015;Available from: http://onlinelibrary.wiley.com/doi/10.1002/mds.26253/pdf.

16. Rosin B, Slovik M, Mitelman R, Rivlin-Etzion M, Haber SN, Israel Z, et al. Closed-Loop Deep Brain Stimulation Is Superior in Ameliorating Parkinsonism. Neuron. 2011 October;72(2):370–384. Available from: http://www.sciencedirect.com/science/article/pii/S0896627311007768.

17. Guitchounts G, Markowitz JE, Liberti WA, Gardner TJ. A carbon-fiber electrode array for long-term neural recording. Journal of Neural Engineering. 2013;10(4). Available from: http://www.ncbi.nlm.nih.gov/pmc/articles/PMC3875136/.

18. Cogan SF. Neural Stimulation and Recording Electrodes. Annual Review of Biomedical Engineering. 2008;10(1):275–309. PMID: 18429704. Available from: http://dx.doi.org/10.1146/annurev.bioeng.10.061807.160518.

19. Long MA, Jin DZ, Fee MS. Support for a synaptic chain model of neuronal sequence generation. Nature. 2010 October;468(7322):394–399. Available from: http://www.ncbi.nlm.nih.gov/pmc/articles/PMC2998755/.

20. Hahnloser RHR, Kozhevnikov AA, Fee MS. An ultra-sparse code underliesthe generation of neural sequences in a songbird. Letters to Nature. 2002 September;419:65–70. Available from: http://www.nature.com/nature/journal/v419/n6902/full/nature00974.html.

21. Swadlow HA. Neocortical efferent neurons with very slowly conducting axons: strategies for reliable antidromic identification. Journal of Neuroscience Methods. 1998 February;79(2):131–141. Available from: http://www.sciencedirect.com/science/article/pii/S0165027097001763#BIB51.

22. Fee MS, Kozhevnikov AA, Hahnloser RHR. Neural Mechanisms of Vocal Sequence Generation in the Songbird. Ann NY Acad Sci. 2004;1016:153–170. Available from: http://web.mit.edu/feelab/publications/Fee%20et%20al%20NYAS%202004.pdf.

23. Histed MH, Bonin V, Reid RC. Direct activation of sparse, distributed populations of cortical neurons by electrical microstimulation. Neuron. 2009 August;63(4):508–522. Available from: http://www.ncbi.nlm.nih.gov/pmc/articles/PMC2874753/.